MNPs-TBAN as a Novel Basic Nanostructure and Efficient Promoter for the Synthesis of Pyranopyrimidinones

E. Khalili[a], N. Ahadi[a] and M.A. Bodaghifard[a,b,]*

[a]*Department of Chemistry, Faculty of Science, Arak University, Arak 38156-88138, Iran*
[b]*Institute of Nanosciences & Nanotechnology, Arak University, Arak, Iran*

(Received 12 August 2020, Accepted 15 December 2020)

In this study, magnetite nanoparticles (Fe_3O_4) were synthesized as a magnetic core by chemical co-precipitation process and coated with a silica layer. The (Fe_3O_4@SiO_2) core-shell magnetic nanoparticles were functionalized by organic-base tags to produce the MNPs-TBAN nanoparticles as a novel hybrid nanostructure. The morphology, stability, and magnetism of this hybrid nanostructure were characterized and studied by Fourier transform infrared spectroscopy (FT-IR), thermal gravimetric analysis (TGA), vibrating sample magnetometry (VSM), X-ray powder diffraction analysis (XRD), scanning electron microscopy (FE-SEM), and transmission electron microscopy (TEM). The prepared hybrid nanomaterial was successfully used as a basic heterogeneous catalyst for the synthesis of pyrano[2,3-*d*]pyrimidine derivatives, *via* the condensation of an aldehyde, malononitrile and barbituric acid or thiobarbituric acid. The reaction was afforded the desired products in high purity and has advantages of excellent yields, simple workup procedure, and short reaction time. The catalyst was easily separated from the reaction mixture with the assistance of an external magnet and reused for several runs without noticeable deterioration in catalytic activity.

INTRODUCTION

Multicomponent reactions (MCR) have been used as an effective method to synthesize a wide range of products and heterocyclic compounds. Multi-component reactions, in comparison with multi-step syntheses and different methods of classical chemistry, have many advantages such as low reaction times, diminished work-up procedures, no use of different solvents, high efficiency, being cheap, and high selectivity, leading to the low environmental impact of MCRs [1,2].

The pyrimidine derivatives have biological and pharmacological properties such as antimicrobial [3], antibacterial [4,5], antimalarial [6] and sedative agents [7]. Also, synthetic compounds containing the barbituric acid moiety in their structure have diverse pharmaceutical and industrial applications. Pyrano[2,3-*d*]pyrimidine derivatives

are used as antitumour [8], cardiotonic [9], hepatoprotective [9], antibronchitic [10] and antifungal agents [11]. In recent years, many catalysts and various methods have been reported for the synthesis of pyrano-pyrimidine derivatives. However, these methods have some disadvantages including long reaction times, harsh reaction conditions, use of homogeneous and toxic catalysts or solvents and boring work-up procedures [12-19]. To avoid these limitations, scientists have intensely focused on developing clean, efficient and facile processes and reusable catalysts for the synthesis of these pharmaceutically important pyrano[2,3-*d*]pyrimidines.

The nanoparticles have high surface areas and do not have more of the above-mentioned disadvantages. Magnetic nanoparticles have also attracted much attention because of their unique properties such drug delivery [20], magnetic resonance imaging [21,22], data storage [23] and being used as easily separable catalysts in organic reactions [24,25]. However, magnetic nanoparticles can easily aggregate into

---

*Corresponding author. E-mail: m-bodaghifard@araku.ac.ir

larger clusters. Besides, they have other deficiencies such as leaching under acidic conditions and being susceptible to autoxidation and toxicity. Therefore, it is necessary to protect the surface of MNPs to reduce these undesirable features. For this purpose, MNPs are usually coated with a polymeric or inorganic matrix [26]. Among inorganic compounds, SiO_2 can be a suitable candidate for protecting the surface of MNPs due to its high chemical and thermal stability and most importantly its easy modification by a wide range of functional groups which increase the chemical and colloidal stability of these compounds [25,27-32]. Besides, using magnetic nanoparticles as catalysts is associated with other advantages including easy synthesis and functionalization, low toxicity, low cost, high activity, and selectivity [25,27-34].

As a part of our continuous effort to develop the green organic reactions and efficient heterogeneous magnetic nanocatalysts [25,35-42], herein we have reported the preparation of a novel heterogeneous and hybrid nanomaterial as an impressive and efficient catalyst for the synthesis of pyrano-pyrimidine derivatives (Scheme 2). The proposed method has a considerable efficiency for a catalyst and environmental compatibility. Also, the catalyst is inexpensive and highly efficient and could be easily recovered and reused.

EXPERIMENTAL

All chemicals were purchased from Merck or Acros chemical companies and used without further purification. Melting points were measured by using capillary tubes on an electrothermal digital apparatus and are uncorrected. Known products were identified by comparison of their spectral data and melting points with those reported in the literature. Thin-layer chromatography (TLC) was performed on UV active aluminum backed plates of silica gel (TLC Silica gel 60 F254). ^1H and ^{13}C NMR spectra were recorded on a Bruker Avance 300 MHz spectrometer at 300 MHz and 75 MHz, respectively. Coupling constants, *J*, were reported in hertz unit (Hz). IR spectra were recorded on a Unicom Galaxy Series FT-IR 5030 spectrophotometer using KBr pellets and are expressed in cm^{-1}. Elemental analyses were performed by Vario EL equipment at Arak University. X-ray diffraction (XRD) was performed on Philips XPert (Cu-Kα
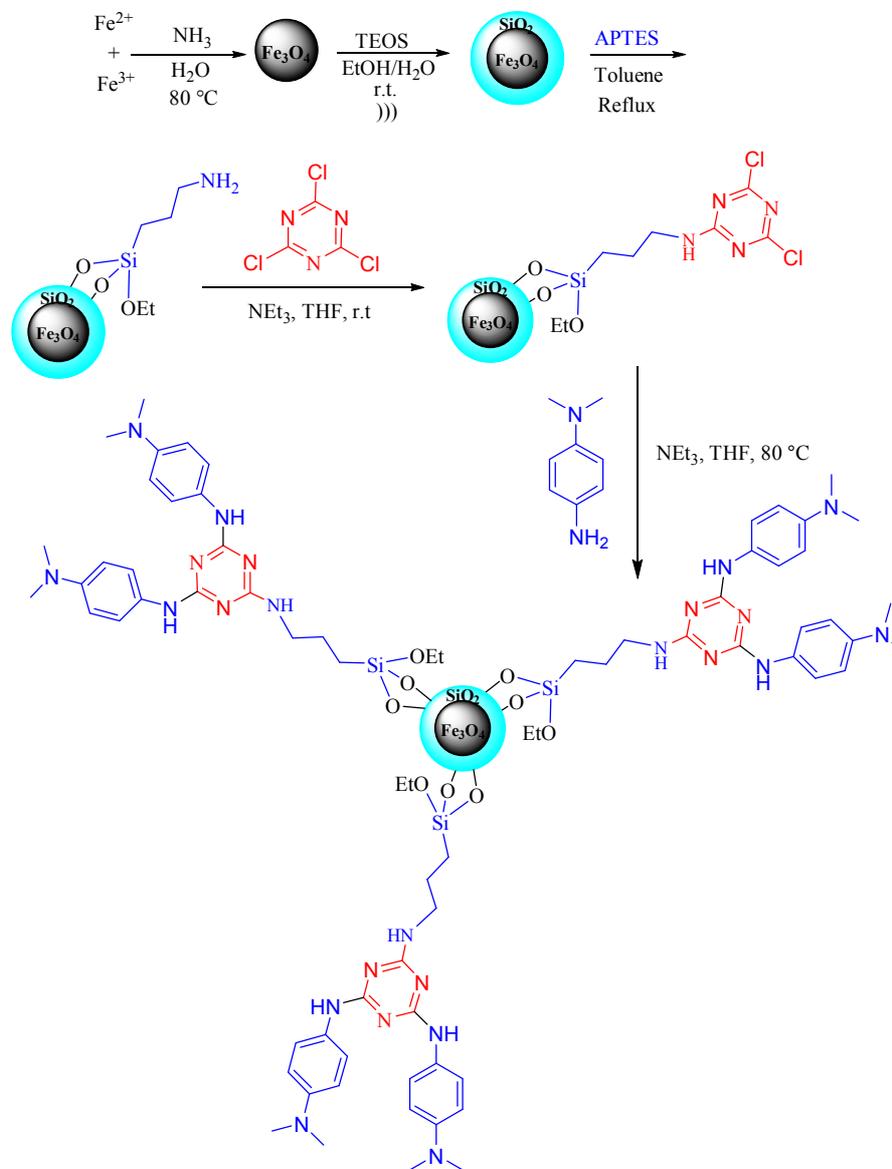
radiation, λ = 0.15405 nm) over the range 2θ = 20-80° using 0.04° as the step length. Thermal gravimetric analysis (TGA) and differential thermal gravimetric (DTG) data for MNPs-TBAN were recorded on a Mettler TA4000 system under the N_2 atmosphere at a heating rate of 10 °C min^{-1}. The scanning electron microscope measurement was carried out on a Hitachi S-4700 field emission-scanning electron microscope (FE-SEM).

Preparation of MNPs-TBAN

Fe_3O_4 MNPs were prepared using chemical co-precipitation of Fe^{3+} and Fe^{2+} ions as described in the literature [43]. The $Fe_3O_4@SiO_2$ core-shell nanoparticles were prepared using the Stöber method [44]. Aminopropyl-modified silica-coated MNPs were prepared according to a reported procedure [45]. Triethylamine (5 mmol, 0.7 g) and triazine trichloride (5 mmol, 0.95 g) were added to a mixture of oven-dried $Fe_3O_4@SiO_2$-$PrNH_2$ MNPs (1 g) in 10 ml THF at 100 ml round-bottomed flask. The reaction mixture was stirred at room temperature for 24 h. The resulting solid was washed with hot THF and dried in an oven to afford the MNPs-TDCl$_2$. MNPs-TDCl$_2$ (1 g) was added to a solution of 4-(dimethylamino)aniline (9.36 mmol, 1.27 g) and triethylamine (9.36 mmol, 1.24 g) in THF (20 ml). The reaction mixture was stirred at 80 °C for 12 h. After completion of the reaction, the resulting solid (MNPs-TBAN) was separated with a magnet, and then washed with hot ethanol and dried in an oven under vacuum (Details in SI).

General Procedure for the Synthesis of Pyrano[2,3-*d*]pyrimidine Derivatives

MNPs-TBAN (0.02 g) was added as a catalyst to a mixture of barbituric acid (1 mmol, 0.128 g) or thiobarbituric acid (1 mmol, 0.144 g), aldehyde (1 mmol), and malononitrile (1 mmol, 0.066 g). The mixture was stirred in solvent-free condition on a preheated oil bath at 100 °C for an appropriate time (Table 1). The progress of the reaction was monitored by TLC. After completion of the reaction, the reaction mixture was diluted with hot DMF (5 ml). The catalyst was easily removed from the reaction mixture using an external magnet. The water was added to the mixture and the separated crude solid product was recrystallized and dried in a vacuum oven.

Scheme 1. Preparation of bis(4-(dimethylamino)anilino)triazine-grafted on silica-coated nano-Fe_3O_4 particles (MNPs-TBAN)

RESULTS AND DISCUSSION

Preparation and Characterization of Hybrid Nanomaterial (MNPs-TBAN)

The MNPs-TBAN as a new and recoverable hybrid nanostructure was constructed *in* five steps from commercially available materials as shown in Scheme 1. Magnetite Fe_3O_4 nanoparticles were prepared by the simple co-precipitation method in basic solution [43]. Considering

the aggregation tendency of the magnetic Fe_3O_4 nanoparticles and to increase their stability, the synthesized Fe_3O_4 nanoparticles were coated by the silica layer using a sol-gel process [44]. The $Fe_3O_4@SiO_2$ core-shell nanostructure was then treated with 3-aminopropyl-triethoxysilane (APTES) which can bind covalently to the free hydroxyl groups (-OH) at the surface of the particles to obtain 3-aminopropyl-grafted magnetic nanoparticles ($Fe_3O_4@SiO_2$-$PrNH_2$) [45]. The subsequent reaction of

Fe_3O_4@SiO_2-$PrNH_2$ with cyanuric chloride was afforded the MNPs-$TDCl_2$ particles. The bis(4-(dimethylamino) anilino)triazine-grafted on silica-coated magnetite nanoparticles (MNPs-TBAN) as the final hybrid nanostructure was obtained by the nucleophilic aromatic substitution reaction of MNPs-$TDCl_2$ and pre-prepared 4-(dimethylamino)aniline. The final hybrid nanomaterial was separated and washed with hot THF and ethanol and then dried in a vacuum oven at 80 °C.

The prepared basic hybrid nanostructure (MNPs-TBAN) was characterized and identified by the Fourier transform infrared spectroscopy (FT-IR), thermal gravimetric analysis (TGA), vibrating sample magnetometry (VSM), X-ray powder diffraction analysis (XRD), scanning electron microscopy (FE-SEM), and transmission electron microscopy (TEM) techniques.

The FT-IR spectroscopy was used to corroborate the successful attachment of different functional groups in each step of the functionalization process. The Fig. 1 shows the FT-IR spectra of Fe_3O_4, Fe_3O_4@SiO_2, Fe_3O_4@SiO_2-$PrNH_2$, Fe_3O_4@SiO_2-$TDCl_2$ and MNPs-TBAN in the wavenumber range 400-4000 cm^{-1}. The FT-IR spectrum of the bare magnetic Fe_3O_4 nanoparticles demonstrated the characteristic Fe-O absorption band around 580 cm^{-1} (Fig. 1a). The Fe_3O_4@SiO_2 spectrum shows characteristic bands at around 1075, 949, 804 and 462 cm^{-1} that are appointed to the asymmetric stretching, symmetric stretching, in-plane bending and rocking mode of the Si-O-Si group, respectively. The broad band in the range 3200-3500 cm^{-1} (stretching vibration mode of Si-OH) and the weak band at 1616 cm^{-1} (twisting vibration mode of H-O-H adsorbed in the silica layer) appeared in the spectrum. These results confirm the formation of SiO_2 shell on the magnetite core. The presence of the grafted alkylamino groups was corroborated by the weak symmetric and asymmetric stretching vibrations at 2920 and 2945 cm^{-1} of aliphatic C-H in Figs. 1c-e. Also, the bands corresponding to C=N and C=C in heterocyclic rings appeared at 1400-1600 cm^{-1} (Fig. 1e). N-H bending vibration appeared at the range 1650 cm^{-1} (Fig. 1e). Therefore, the above results confirm that the functional groups were successfully grafted onto the surface of the magnetic Fe_3O_4@SiO_2 nanoparticles and resulted the final MNPs-TBAN hybrid nanostructure.

The morphology and size of the synthesized nanoparticles were ascertained by the field emission scanning electron microscopy (FE-SEM) (Fig. 2). As shown in Fig. 2, the MNPs-TBAN particles possess nearly spherical morphology with an average diameter of about 20-35 nm. Due to the small size of the particles, the ratio of the surface to the volume of these particles is high, so more contacts with the reactants take place, indicating a well-performed catalytic activity.

The energy-dispersive X-ray spectroscopy (EDS) results, obtained from SEM analysis of MNPs-TBAN, are shown in Fig. 3, and clearly display the presence of Fe, Si, O, N and C in the MNPs-TBAN (Fig. 3). Besides, the higher peak intensity of the Si element compared to Fe peak indicates that Fe_3O_4 nanoparticles are trapped by SiO_2, confirming the synthesized core-shell structure.

The TEM analysis provides additional details on the size and morphology of nanoparticles. The structure of the magnetic nanoparticles MNPs-TBAN is almost spherical. This technique displays a dark nano-Fe_3O_4 core surrounded by a grey silica shell with 5-10 nm thickness and the average size of the synthesized nanoparticles is estimated to be 20-30 nm (Fig. 4).

X-ray powder diffraction (XRD) was used to determine the degree of crystallinity of the magnetite and MNPs-TBAN catalyst (Fig. 5). The same peaks were observed in the XRD patterns of both Fe_3O_4 and MNPs-TBAN, indicating the maintenance of the crystalline spinel ferrite core structure through the functionalization process. The XRD patterns of the synthesized MNPs-TBAN showed diffraction peaks at 2θ = 30.4°, 35.7°, 43.3°, 53.9°, 57.5°, 63° and 74.5° that could be assigned to the (220), (311), (400), (422), (511), (440) and (533) Miller planes of Fe_3O_4 nanoparticles. These results match well with the standard Fe_3O_4 sample (JCPDS card no. 85-1436) and confirm that the Fe_3O_4 nanoparticles are pure and have a cubic spinel structure. The broad peak from 2θ = 20° to 27° is consistent with an amorphous silica phase of MNPs-TBAN (Fig. 4b) [46]. The average crystallite size of the MNPs by Scherrer's formula ($D = 0.9\lambda/\beta\cos\theta$) was estimated from the (311) XRD peak [47]. The crystallite size of the MNPs, as calculated from the width of the peak at 2θ = 35.7° (311), was 23.5 nm, in the range determined by FE-SEM and TEM analyses (Figs. 2 and 4).
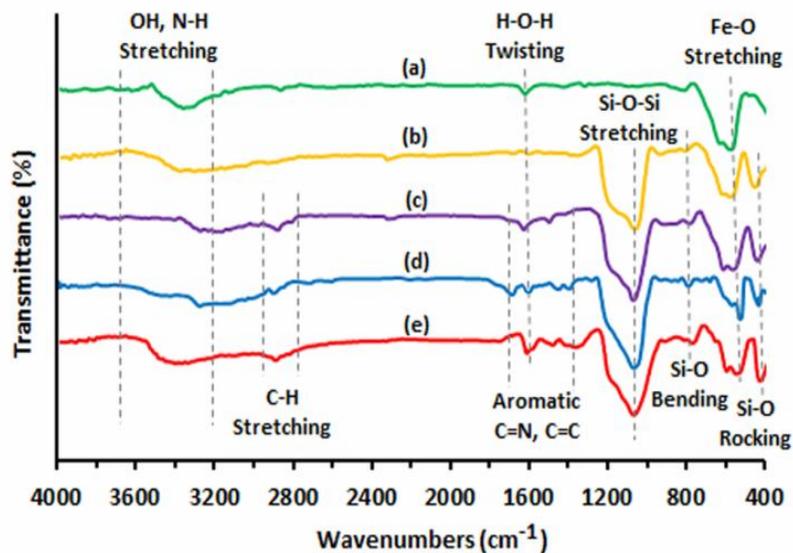
Fig. 1. The FT-IR spectra for (a) Fe_3O_4, (b) $Fe_3O_4@SiO_2$, (c) $Fe_3O_4@SiO_2-PrNH_2$, (d) $Fe_3O_4@SiO_2-TDCl_2$ and (e) MNPs-TBAN nanomaterials.
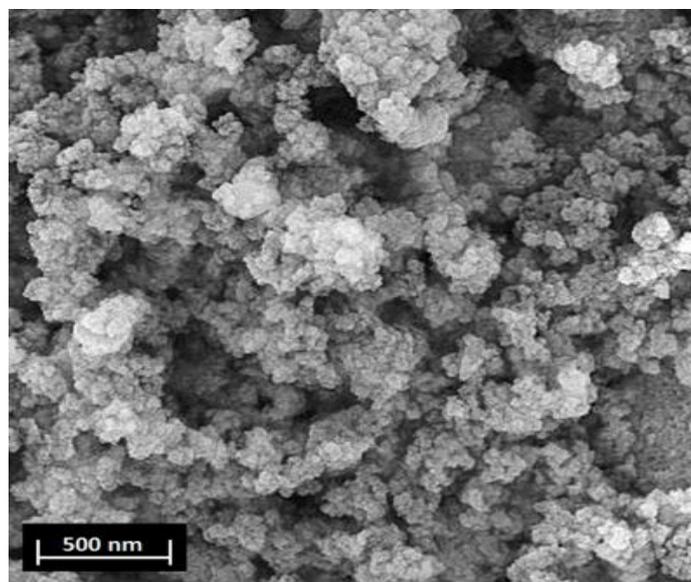

Fig. 2. The FE-SEM images of MNPs-TBAN nanoparticles.

The thermogravimetric analysis (TGA) and derivative thermogravimetry (DTG) were used to determine the stability of the hybrid nanomaterial (Fig. 6). The magnetic catalyst (MNPs-TBAN) displays two steps of weight loss over the temperature range of TGA. The first step, including a low amount of weight loss at T < 250 °C, is due to the removal of physically adsorbed solvent and surface hydroxyl groups; the second stage at about 250 to nearly 590 °C is ascribed to the decomposition of the coating organic moiety in the nanocomposite. Thus, the weight loss
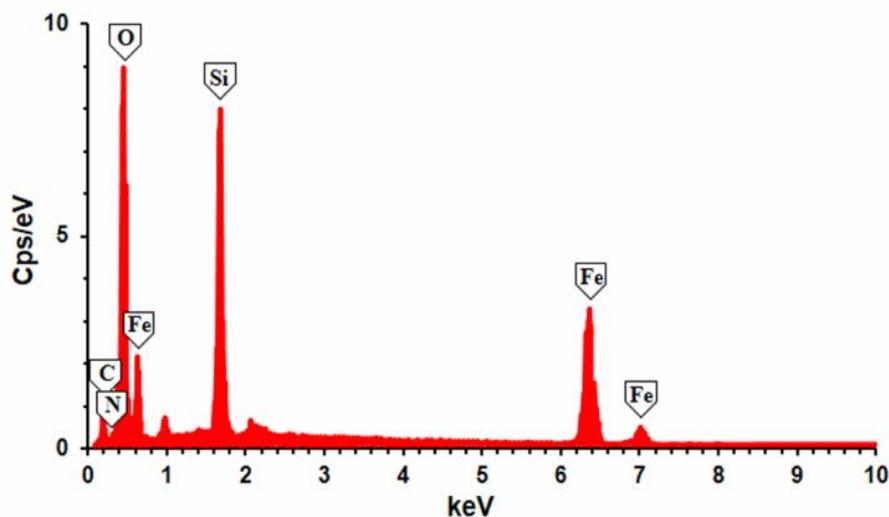
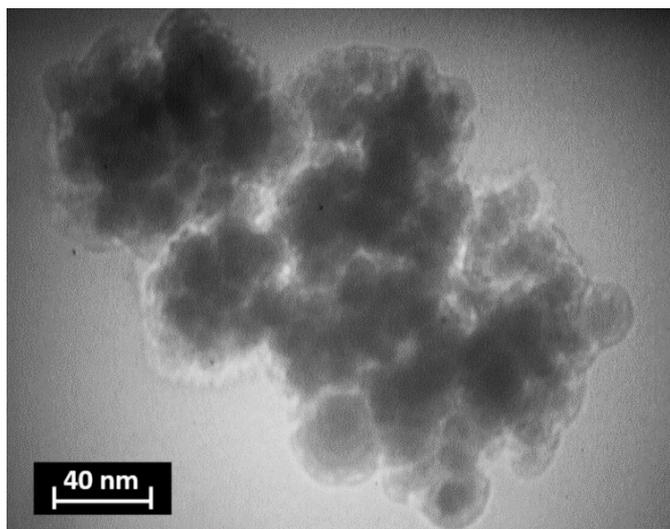**Fig. 3.** The EDS spectrum of MNPs-TBAN nanoparticles.

Fig. 4. The TEM image of MNPs-TBAN nanoparticles.

between 250 and 590 °C gives the organic grafting ratios of the magnetic catalyst. The observed weight loss at 600 °C temperatures and higher is related to the silica nanoparticle groups, which is related to the phase change step. The slope of the curve represents the significant thermal resistance shown by the sample. Therefore, it can be concluded that almost the entire surface of the sample has been functionalized by organic groups. It can be seen from the

DTG chart that the organic structure decomposition has occurred mainly at 690 °C and the catalyst is completely stable at temperatures up to 250 °C.

The magnetic properties of the nanoparticles were characterized using a vibrating sample magnetometer (VSM). Figure 7 shows the plots of room temperature magnetization (*M*) versus magnetic field (*H*) (*M-H* curves or hysteresis loops) of Fe_3O_4 and MNPs-TBAN
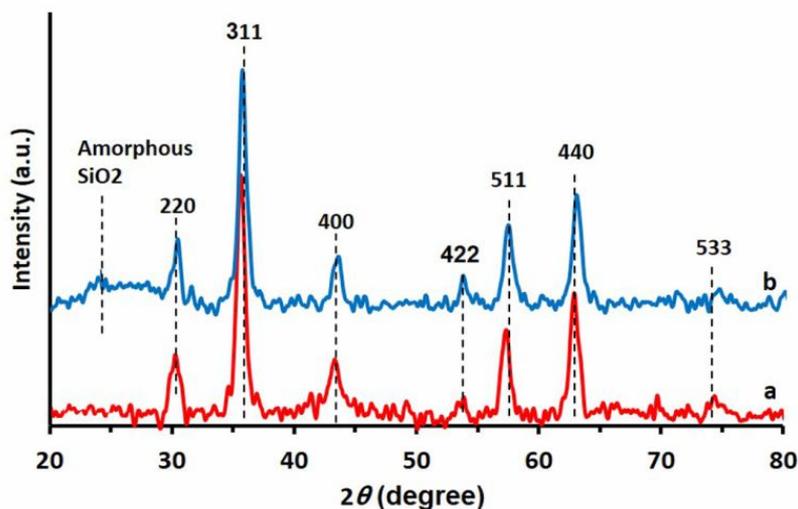
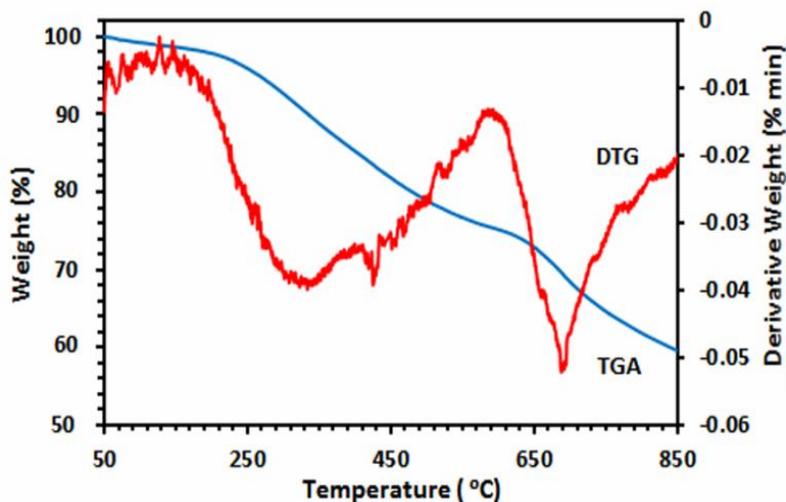**Fig. 5.** The XRD patterns of (a) Fe_3O_4 and (b) MNPs-TBAN.

Fig. 6. The TGA and DTG curves for MNPs-TBAN nanoparticles.

nanoparticles. The hysteresis curve allows determination of the saturation magnetization (M_s), remanent magnetization (M_r) and coercivity (H_c). The magnetization of samples could be completely saturated at high fields of up to ±8000.0 Oe and the M_s of samples changed from 62 to 38 emu g^{-1}, due to the formation of a silica shell around the Fe_3O_4 core. The hysteresis loops show the super-paramagnetic behavior of the Fe_3O_4 and MNPs-TBAN particles in which M_r and H_c are close to zero ($M_r = 2.5$ and

1.5 emu g^{-1}, and $H_c = 16$ and 18 Oe, respectively) [48]. The strong magnetization of the nanoparticles was also revealed by simple attraction with an external magnet (Fig. 7).

Synthesis of Pyrano[2,3-*d*]pyrimidine Derivatives Using MNPs-TBAN

After characterization of the prepared hybrid nanomaterial and to optimize the reaction condition, the reaction of 4-chlorobenzaldehyde (1 mmol), barbituric acid
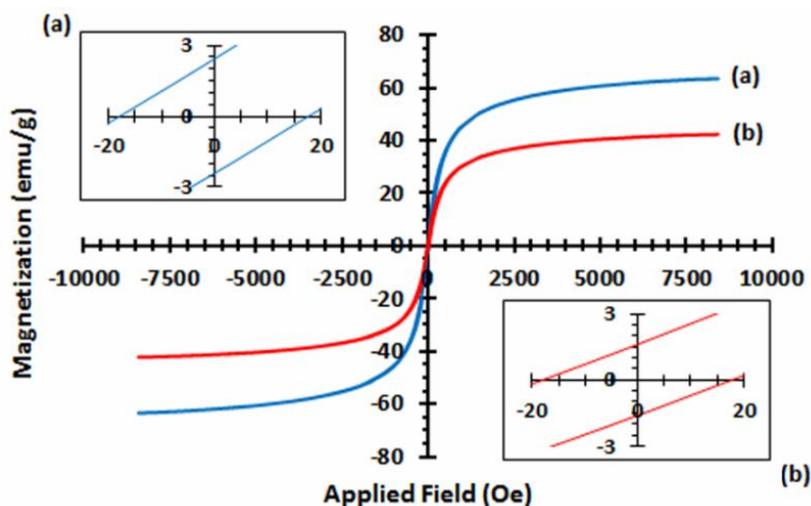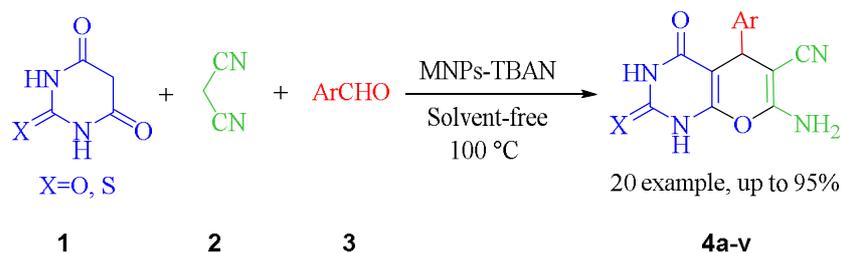
Fig. 7. The magnetic hysteresis loops of Fe_3O_4 MNPs (a) and MNPs-TBAN (b). Left and right inset: the magnified zone from -20 to 20 Oe.
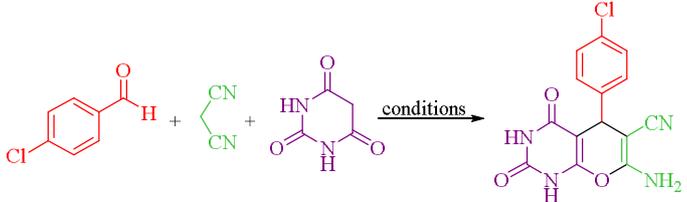

Scheme 2. Multicomponent synthesis of pyrano[2,3-*d*]pyrimidine using bis(4-(dimethylamino)anilino)triazine-grafted on silica-coated magnetite nanoparticles (MNPs-TBAN)

(1 mmol), and malononitrile (1 mmol) were selected as a model and was conducted under different reaction conditions. The best result was obtained using 50 mg of MNPs-TBAN under solvent-free condition at 100 °C, concerning the reaction time and yield of the desired product (Table 1, entry 12). The efficiencies of Fe_3O_4, $Fe_3O_4@SiO_2$, MNPs-PrNH$_2$ and MNPs-TDCl$_2$ as the catalyst toward the model reaction were compared; the results are demonstrated in Table1. It was shown that the MNPs-TBAN was the best choice (Table 1, entries 16-19). Arylaldehyde with both electron-donating or electron-withdrawing groups and heteroaromatic aldehydes can lead to the desired products in good to excellent yields (Table 2). As can be seen in Table 2, the nature of substituents on the

aromatic ring of aldehydes did not show an obvious effect in terms of time and yield under the reaction condition. The comparison of MNPs-TBAN nanocatalyst with some previously reported catalysts for the synthesis of pyrano[2,3-*d*]pyrimidines is shown in Table 3. The presented data confirm that MNPs-TBAN is an efficient and suitable catalyst for the synthesis of desired pyrano[2,3-*d*]pyrimidines derivatives. The spectroscopic data for novel products (4n and 4u) and other selected products (4d, 4f, 4m and 4q) are presented in supplementary information.

The suggested mechanism for the formation of these compounds is presented in Scheme 3. Initially, MNPs-TBAN as a basic catalyst abstracts the acidic hydrogen from malononitrile. The Knoevenagel

Table 1. Optimization of the Conditions for the Synthesis of Pyrano[2,3-*d*]pyrimidine Derivatives

No.	Catalyst (mg)	Solvent	Temp. (°C)	Time (min)	Yield (%)[a]
1	MNPs-TBAN (50)	CH$_3$CN	Reflux	100	73
2	MNPs-TBAN (50)	CH$_2$Cl$_2$	Reflux	100	61
3	MNPs-TBAN (50)	THF	Reflux	100	67
4	MNPs-TBAN (50)	Toluene	Reflux	100	77
5	MNPs-TBAN (50)	H$_2$O	Reflux	60	63
6	MNPs-TBAN (50)	EtOH	Reflux	60	81
7	MNPs-TBAN (50)	EtOH:H$_2$O	Reflux	60	87
9	MNPs-TBAN (50)	Solvent-free	50	100	79
10	MNPs-TBAN (50)	Solvent-free	80	30	89
11	MNPs-TBAN (50)	Solvent-free	100	10	93
12	MNPs-TBAN (20)	Solvent-free	100	10	94
13	MNPs-TBAN (10)	Solvent-free	100	30	87
14	-	Solvent-free	100	100	41
15	Fe$_3$O$_4$ (50)	Solvent-free	100	120	77
16	Fe$_3$O$_4$@SiO$_2$ (50)	Solvent-free	100	120	65
17	MNPs-PrNH$_2$ (50)	Solvent-free	100	120	67
18	MNPs-TDCl$_2$ (50)	Solvent-free	100	120	69

[a]Isolated yield.

condensation *via* nucleophilic attack of the malononitrile anion to the carbonyl group (aromatic aldehyde) and subsequent elimination of water leads to the formation of electrophilic intermediate (A, arylidine malononitrile).

Subsequently, barbiturate nucleophile, barbituric acid that its acidic hydrogen has been abstracted by the catalyst, attacks to electrophilic olefin (Michael addition) to form the adduct B. The resulting product undergoes an isomerization

Table 2. Multicomponent One-pot Synthesis of Pyrano[2,3-d]pyrimidine Derivatives

Product	Ar	X	Time (min)	Yield (%)[a]	M.P. (°C)[b] Found	M.P. (°C)[b] Reported
4a	C_6H_5	O	15	95	219-221	220-222[14]
4b	2-Cl-C_6H_4	O	20	92	209-211	204-206[14]
4c	4-Cl-C_6H_4	O	10	94	239-241	238-240[14]
4d	3-NO_2-C_6H_4	O	15	93	262-264	268-270[13]
4e	4-NO_2-C_6H_4	O	15	91	235-236	239-240[13]
4f	4-Br-C_6H_4	O	10	90	228-230	230-231[13]
4g	4-CH_3-C_6H_4	O	15	91	231-233	225[12]
4h	4-OH-C_6H_4	O	25	89	>300	>300[15]
4i	3-OH-C_6H_4	O	25	87	216-218	202-204[14]
4j	4-OMe-C_6H_4	O	20	91	276-278	280-281[15]
4k	4-N(Me)$_2$-C_6H_4	O	20	89	227-229	207-210[16]
4l	4-F-C_6H_4	O	10	93	223-224	218-220[14]
4m	2,4-Cl_2-C_6H_3	O	15	95	247-249	241-242[13]
4n	Isophthaldehyde	O	20	87	273-275	-
4o	2-Thienyl	O	25	91	265-267	272-273[15]
4p	C_6H_5	S	15	93	215-217	223-224[15]
4q	4-Cl-C_6H_4	S	15	91	>300	>300[15]
4r	3-Cl-C_6H_4	S	15	93	233-234	238-239[15]
4s	4-NO_2-C_6H_4	S	15	90	237-239	234-235[15]
4t	3-NO_2-C_6H_4	S	20	93	228-230	233-234[13]
4u	4-CH_3-C_6H_4	S	30	90	195-197	-
4v	4-OMe-C_6H_4	S	30	90	123-125	116-118[17]

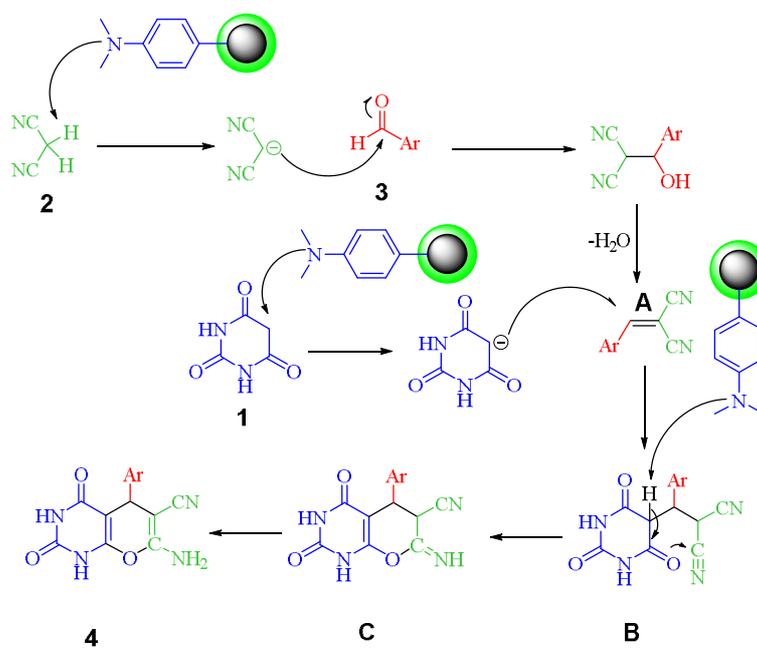[a]Isolated yield. [b]Melting points were not corrected.

to form an enol and intramolecular cycloaddition then occurred to afford an imine adduct (C), which could be tautomerized to give the desired final product (4).

Catalyst Recovery and Reusability

The recovery and reuse of the catalyst are very important for industrial application and compliance with the

Table 3. Comparison of MNPs-TBAN as a Catalyst with some other Reported Catalysts in the Synthesis of Pyrano[2,3-*d*]pyrimidine

Entry	Catalyst	Condition	Time (min)	Yield (%)
1	Zn[(L)proline]$_2$	EtOH, reflux	60	85 [12]
2	DAHP	aq. EtOH, reflux	120	81 [13]
3	DMA	EtOH, reflux	20	90 [14]
4	KBr, electrolysis	H$_2$O:EtOH, r.t	20	79 [16]
5	Choline chloride. ZnCl$_2$, triethanolamine	EtOH, r.t	120	94 [17]
6	[BMIm]BF$_4$	90 °C	180	84 [18]
7	CuCl$_2$.2H$_2$O	H$_2$O:EtOH, 60 °C	35	89 [19]
8	MNPs-TBAN	Solvent-free, 100 °C	15	95 [This work]

Scheme 3. The possible mechanism for the synthesis of pyrano[2,3-*d*]pyrimidine derivatives
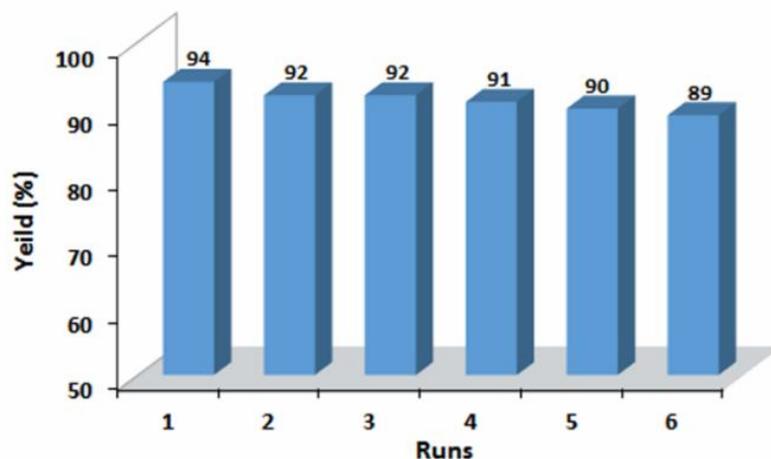
Fig. 8. Recyclability of MNPs-TBAN in the model reaction for the synthesis of pyrano[2,3-d]pyrimidine derivatives.
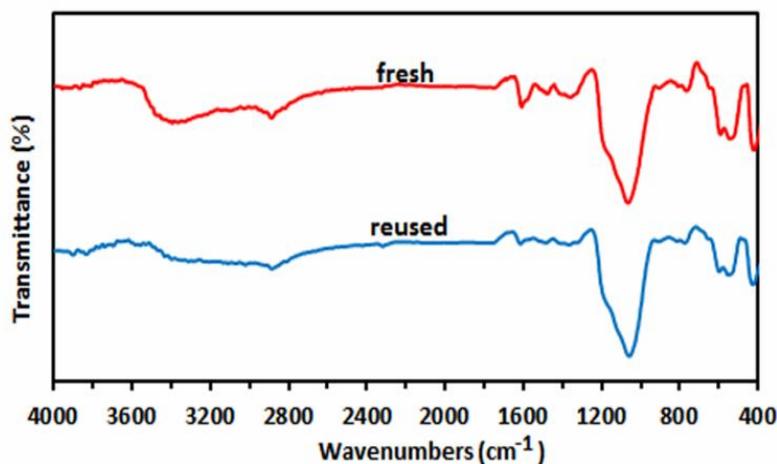

Fig. 9. The FT-IR spectra of the fresh catalyst and the six-times reused catalyst.

principles of green chemistry. The recycling capability of MNPs-TBAN was investigated in the reaction of barbituric acid (1 mmol), 4-chlorobenzaldehyde (1 mmol) and malononitrile (1 mmol) under the solvent-free condition at 100 °C for 10 min. After completion of the reaction, the resulting solidified mixture was diluted with hot DMF (5 ml). Then the catalyst was easily separated using an external magnet, washed with ethanol, dried under vacuum and reused in a subsequent reaction. Nearly quantitative recovery of the catalyst (up to 98%) could be obtained from

each run. As seen in Fig. 8, the recycled catalyst could be reused six times without any additional modifications or a significant decrease in catalytic activity. The recycled catalyst after six runs had no distinct change in structure, as shown by a comparison of the FT-IR spectra to that of fresh catalyst (Fig. 9).

CONCLUSIONS

In this study, the bis(4-(dimethylamino)anilino)triazine-

grafted on silica-coated magnetite nanoparticles (MNPs-TBAN) as a novel hybrid nanostructure was successfully prepared and characterized. The MNPs-TBAN as an efficient basic hybrid nanocatalyst was used in the one-pot multicomponent synthesis of pyrano[2,3-*d*]pyrimidinone derivatives. The desired products were synthesized in high to excellent yields through an easy and green methodology without using harmful solvents (under solvent-free condition). The prepared catalyst can be easily separated and recovered from the reaction system by a magnet and can be reused several times without a significant loss of its activity. Also, this procedure offers several advantages such as clean reaction conditions and minimum pollution of the environment, high yields, short reaction time, and easy separation of the catalyst, that makes it an effective and attractive method for the synthesis of the biologically interesting pyrano-pyrimidine derivatives, comparable with those reported in the literature.

ACKNOWLEDGMENTS

Supplementary Materials

Supplementary materials are available on the publisher's website along with the manuscript and contain the spectroscopic and characterization data for products and prepared MNPs-TBAN.

REFERENCES

[1]   G. Guillena, D.J. Ramon, M. Yus, Tetrahedron: Asymmetry 18 (2007) 693.

[2]   R.C. Cioc, E.E. Ruijter, R.V. Orru, Green Chem. 16 (2014) 2958.

[3]   M.R. Shaaban, Heterocycles 75 (2008) 3005-3014.

[4]   H. Goker, G.A, Kilcigil, M. Tuncbilek, C. Kus, Heterocycles 51 (1999) 2561.

[5]   P. Černuchová, G. Vo-Thanh, V. Milata, A. Loupy, S. Jantová, M. Theiszová, Tetrahedron 61 (2005) 5379.

[6]   L.M. Werbel, A. Curry, E.F. Elslager, C.A. Hess, J. Heterocycl. Chem. 6 (1969) 787.

[7]   A. Kreutzberger, M. Leger, Arch. Pharm. 316 (1983) 582.

[8]   E.M. Grivaky, S. Lee, C.W. Siyal, D.S. Duch, C.A. Nichol, J. Med. Chem. 23 (1980) 327.

[9]   D. Heber, C. Heers, U. Ravens, Die Pharmazie 48 (1993) 537.

[10] A. Pałasz, Monatsh. Chem. 139 (2008) 1397.

[11] A.R. Bhat, R.S. Dongre, R.S. Selokar, Int. J. Pharma. Bio. Sci. 5 (2014) 422.

[12] M.M. Heravi, A. Ghods, K. Bakhtiari, F. Derikvand, Synth. Commun. 40 (2010) 1927.

[13] S. Balalaie, S. Abdolmohammadi, H.R. Bijanzadeh, A.M. Amani, Mol. Divers. 12 (2008) 85.

[14] R. Ramesh, A. Lalitha, Res. Chem. Int. 41 (2015) 8009.

[15] M. Kidwai, A. Jain, S. Bhardwaj, Mol. Divers. 16 (2012) 121.

[16] H. Kefayati, M. Valizadeh, A. Islamnezhad, Anal. Bioanal. Electrochem. 6 (2014) 80.

[17] D.K. Yadav, M.A. Quraishi, J. Mater. Environ. Sci. 5 (2014) 1075.

[18] J. Yu, H. Wang, Synth. Commun. 35 (2005) 3133.

[19] M.T. Maghsoodlou, F. Mohamadpour, M. Lashkari, N. Hazeri, Org. Chem. Res. 4 (2018) 140.

[20] J. Dobson, Drug Dev. Res. 67 (2006) 55.

[21] S. Mornet, S. Vasseur, F. Grasset, P. Verveka, G. Goglio, A. Demourgues, J. Portier, E. Pollert, E. Duguet, Prog. Solid State Chem. 34 (2006) 237.

[22] Z. Li, L. Wei, M.Y. Gao, H. Lei, Adv. Mater. 17 (2005) 1001.

[23] T. Hyeon, Chem. Commun. 8 (2003) 927.

[24] F. Rezaei, M.A. Amrollahi, R. Khalifeh, Chem. Select 5 (2020) 1760.

[25] M.A. Bodaghifard, M. Hamidinasab, N. Ahadi, Curr. Org. Chem. 22 (2018) 234.

[26] S.H. Araghi, M.H. Entezari, Appl. Surf. Sci. 333 (2015) 68.

[27] M.B. Gawande, P.S. Branco, R.S. Varma, Chem. Soc. Rev. 42 (2013) 3371.

[28] J.A. Gladyzs, Chem. Rev. 102 (2002) 3215.

[29] V. Polshettiwar, R. Luque, A. Fihri, H. Zhu, M. Bouhrara, J.M. Basset, Chem. Rev. 111 (2011) 3036.

[30] S. Shylesh, V. Schünemann, W.R. Thiel, Angew. Chem. Int. Edit. 49 (2010) 3428.

[31] Y. Leng, K. Sato, Y. Shi, J.G. Li, T. Ishigaki, T. Yoshida, H. Kamiya, J. Phys. Chem. C 113 (2009) 16681.

[32] A.L. Morel, S.I. Nikitenko, K. Gionnet, A. Wattiaux, J. Lai-Kee-Him, C. Labrugere, B. Chevalier, G. Deleris, C. Petibois, A. Brisson, M. Simonoff, ACS Nano 2 (2008) 847.

[33] M. Esmaeilpour, A.R. Sardarian, J. Javidi, Appl. Catal. A 445 (2012) 359.

[34] M.R. Shafiee, M. Ghashang, A. Fazlinia, Curr. Nanosci. 9 (2013) 197.

[35] N. Foroughifar, A. Mobinikhaledi, S. Ebrahimi, M.A. Bodaghi Fard, H. Moghanian, J. Chin. Chem. Soc. 56 (2009), 1043.

[36] A. Mobinikhaledi, M. Zendehdel, M. Hamidi Nasab, M.A. Bodaghi Fard, Heterocyc. Commun. 15 (2009) 451.

[37] M.A. Bodaghifard, A. Mobinikhaledi, M. Hamidinasab, Synth. React. Inorg. Met.-Org. Nano-Metal. Chem. 44 (2014) 567.

[38] M.A. Bodaghifard, Z. Faraki, A.R. Karimi, Curr. Org. Chem. 20 (2016) 1648.

[39] N. Ahadi, M.A. Bodaghifard, A. Mobinikhaledi, Appl. Organomet. Chem. 33 (2019) e4738.

[40] S. Asadbegi, M.A. Bodaghifard, E. Alimohammadi, R. Ahangarani-Farahani, Chem. Select 3 (2018) 13297.

[41] H. Moghanian, M.A. Bodaghifard, A. Mobinikhaledi, N. Ahadi, Res. Chem. Int. 44 (2018) 4083.

[42] M.A. Bodaghifard, J. Organomet. Chem. 886 (2019) 57.

[43] K. Can, M. Ozmen, M. Ersoz, Colloids Surf. B Biointerfaces 71 (2009) 154.

[44] W. Stöber, A. Fink, E. Bohn, J. Colloid Interface Sci. 26 (1968) 62.

[45] T. Zeng, L. Yang, R. Hudson, G. Song, A.R. Moores, C.J. Li, Org. Lett. 13 (2010) 442.

[46] G. Feng, D. Hu, L. Yang, Y. Cui, X.A. Cui, H. Li, Sep. Purif. Technol. 74 (2010) 253.

[47] J. Giri, S.G. Thakurta, J. Bellare, A.K. Nigam, D. Bahadur, J. Magn. Magn. Mater. 293 (2005) 62.

[48] K. Petcharoen, A. Sirivat, Mater. Sci. Eng. B 177 (2012) 421.